Relaxation and domain formation in incommensurate two-dimensional heterostructures

Stephen Carr, Daniel Massatt, Steven B. Torrisi, Paul Cazeaux, Mitchell Luskin, and Efthimios Kaxiras

Phys. Rev. B **98**, 224102 — Published 5 December 2018

DOI: 10.1103/PhysRevB.98.224102

Relaxation and Domain Formation in Incommensurate 2D Heterostructures

Stephen Carr,[1] Daniel Massatt,[2] Steven B. Torrisi,[1] Paul Cazeaux,[3] Mitchell Luskin,[2] and Efthimios Kaxiras[1,4]

[1]*Department of Physics, Harvard University, Cambridge, Massachusetts 02138, USA.*
[2]*School of Mathematics, University of Minnesota, Minneapolis, Minnesota, 55455, USA.*
[3]*Department of Mathematics, University of Kansas, Lawrence, Kansas, 66045, USA.*
[4]*John A. Paulson School of Engineering and Applied Sciences, Harvard University, Cambridge, Massachusetts 02138, USA.*

(Dated: October 31, 2018)

We introduce configuration space as a natural representation for calculating the mechanical relaxation patterns of incommensurate two-dimensional (2D) bilayers. The approach can be applied to a wide variety of 2D materials through the use of a continuum model in combination with a generalized stacking fault energy for interlayer interactions. We present computational results for small-angle twisted bilayer graphene and molybdenum disulfide (MoS_2), a representative material of the transition metal dichalcogenide (TMDC) family of 2D semiconductors. We calculate accurate relaxations for MoS_2 even at small twist-angle values, enabled by the fact that our approach does not rely on empirical atomistic potentials for interlayer coupling. The results demonstrate the efficiency of the configuration space method by computing relaxations with minimal computational cost. We also outline a general explanation of domain formation in 2D bilayers with nearly-aligned lattices, taking advantage of the relationship between real space and configuration space. The configuration space approach also enables calculation of relaxations in incommensurate multilayer systems.

Layered materials consist of 2D atomically thin sheets which are weakly coupled by the van der Waals force. For understanding the electronic and mechanical properties of multilayered structures of such materials, it is useful to view them as a series of conventional crystals with a weak perturbative interaction between sheets[1]. Bilayer systems with slight lattice misalignment due to differing lattice constants or relative twist-angle are of interest in optical and transport experiments[2–5]. In small-angle twisted bilayer graphene (tBLG) and graphene-hBN bilayers, highly regular domain-wall patterns have been observed experimentally and studied theoretically[6–9] and have been attributed to the general strain-soliton phenmenon[10–12]. The appearance of domain walls is the result of atomic relaxation which serves to minimize the additional energy due to misalignment. Under electric-field gating the domain walls give rise to interesting topologically-protected edge states[13–18]. Understanding this relaxation and predicting its behavior in other nearly-aligned bilayers may be useful in the search for topological edge states and quantum information applications.

We study three different bilayer systems, graphene and the two high-symmetry alignments of MoS_2, which is a standard representative of the transition-metal dichalcogenide family of 2D materials. Bilayer graphene and graphene-hBN systems have been modeled with a continuum approach[8,19,20], where the discrete atomic positions are replaced by a continuous field of displacements. These real space continuum approaches work well in the case of a twisted bilayer because any bilayer moiré pattern becomes periodic in the continuum limit. However not every incommensurate system is periodic in a continuum limit. As an example, consider a three layer system which is mutually incommensurate (e.g. all three of the layers' unit cells are linearly independent). Letting Γ_{ij} be the bilayer moiré cell generated by layers i and j, then Γ_{12} and Γ_{23} are not guaranteed to form a periodic supercell. This is not a statement about atomistic commensurability, but rather commensurability of a pure continuum model. From this perspective, we argue that existing continuum models developed for twisted bilayers may not be easily extended with full generality to multilayer systems.

To address this problem, we revisit the bilayer continuum relaxation problem but introduce a different approach: consider minimizing total energy over a collection of all possible local atomic environments, which we call configuration space[21]. In brief, every atomic site in a real space bilayer structure has a corresponding local environment that describes the relative stacking disregistry. A construction of configuration space is outlined in Fig. 1, and is explained more precisely later in the text. We introduce the formalism of configuration space here and discuss some of the challenges of the multilayer problem, but leave the multilayer implementation to a future work. We find that in the twisted bilayer case the configuration space methodology reduces to existing real space continuum models up to a change of variables while providing a different physical insight. The bilayer relaxation patterns in configuration space show high energy stacking environments "flowing" to low energy, a phenomenon that is not as obvious in real space relaxation patterns.

To begin, we summarize the common continuum approach to bilayer relaxation in real space before generalizing it for configuration space. It is convenient to separate the energy into interlayer (stacking) and intralayer (strain) energy, as the two layers weakly interact with one another. We will assume smooth and slowly-varying relaxation in each layer, described by a position-dependent displacement vector field $\mathbf{U}_i(r)$ where i indexes the layer number. We will only consider in-plane

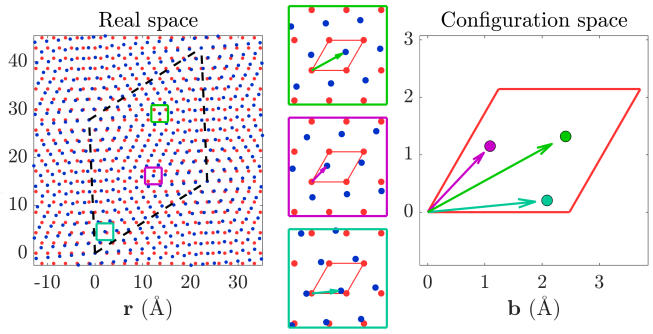

FIG. 1. How to map the atomic degrees of freedom of a moiré cell in real space to configuration space. Two triangular lattices (red and blue) are twisted relative to one another, forming a moiré pattern (dashed black line). Three blue atoms are highlighted in cyan, purple, and green, and their stacking relative to the underlying red lattice is shown in the boxed insets. These environments are described by vectors that lie within the unit-cell of the red layer, allowing one to translate every atom in real space to a specific point **b** in configuration space.

relaxation, which is appropriate for a bilayer encapsulated in a stiff substrate, although the method can be extended for out-of-plane relaxations as well. Such encapsulated systems show improved optical and electronic transport properties[22] and are of great experimental interest.

Under these assumptions, the intralayer energy for a layer is well described by a linear isotropic continuum approximation

$$\begin{aligned} E_{\text{intra}} &= \lim_{R\to\infty} \frac{1}{|B_R|} \int_{B_R} \frac{1}{2}\mathcal{E}\left(\nabla \mathbf{U}_i\right)\ C_i\ \mathcal{E}\left(\nabla \mathbf{U}_i\right) dr \\ &= \lim_{R\to\infty} \frac{1}{|B_R|} \int_{B_R} \frac{1}{2}\Big[K_i(\partial_x U_{ix} + \partial_y U_{iy})^2 + \\ &\quad G_i((\partial_x U_{ix} - \partial_y U_{iy})^2 + (\partial_x U_{iy} + \partial_y U_{ix})^2)\Big] dr \end{aligned} \tag{1}$$

where $\mathcal{E}(\nabla \mathbf{U}_i) = \frac{1}{2}(\nabla \mathbf{U}_i + \nabla \mathbf{U}_i^T)$ is the 2×2 infinitesimal strain tensor and B_R is a sphere of radius R used to normalize the integral. The fourth-order stiffness tensor C depends on the two parameters K (bulk modulus) and G (shear modulus) which represent the energy cost associated with strain. This approximation does not capture short-range symmetry-breaking effects like Peierls distortions, but can describe the long-range domain-walls observed in twisted bilayer graphene.

For the interlayer energy, we use the generalized stacking fault energy (GSFE) surface. This concept was originally used to describe the energy of defects in bulk crystals[23–26] and has recently been employed for explaining relaxation in graphene and hBN bilayers[27,28]. The GSFE provides the interlayer energy per unit cell and depends only on the relative stacking between two successive layers. We denote this functional by V_{GSFE}, with the initial local stacking configuration between layers given by the 2D vector $\mathbf{b}(\mathbf{r})$. We can obtain the stacking after relaxation by adding in the displacement fields $\mathbf{U}_i(\mathbf{r})$, giving a normalized interlayer energy:

$$E_{\text{inter}} = \lim_{R\to\infty} \frac{1}{|B_R|} \int_{B_R} V_{\text{GSFE}}(\mathbf{b}(\mathbf{r}) + \mathbf{U}_1(\mathbf{r}) - \mathbf{U}_2(\mathbf{r}))d\mathbf{r}. \tag{2}$$

These intralayer and interlayer couplings are obtained from total-energy calculations based on density-functional theory (DFT) with the Vienna Ab initio Simulation Package (VASP)[29,30]. A unit-cell with basis vectors $\mathbf{a_1} = a(1,0)$ and $\mathbf{a_2} = a(\sqrt{3}/2, 1/2)$ is used, where the lattice parameter a for graphene is 2.47 Å and for MoS_2 is 3.18 Å . For the intralayer coupling, isotropic and anisotropic strain are applied to an optimized monolayer unit cell, distorting the x and y axes by $\pm 1.5\%$ in steps of 0.3%. We obtain K and G of Eq. (1) by linear fitting of the ground-state energy dependence on this applied strain. For MoS_2, the sulfur atom heights for each strain sample are relaxed while calculating the ground-state energy.

For the interlayer GSFE, we use previously reported DFT results for bilayer graphene stacking[27]. In MoS_2, the GSFE was parameterized by evaluating the energy on a grid of points for an MoS_2 bilayer, with the van der Waals force implemented through the vdW-DFT method using the SCAN+rVV10 functional[31,32]. The in-plane positions of all atoms in the bilayer are fixed but they are allowed to relax in the out-of-plane direction. The top layer is shifted relative to the bottom layer over a 9×9 grid in the unit cell to sample the GSFE energy landscape. To fit the V_{GSFE} to this set of values, we use a form similar to that used by Zhou et. al.[27], but with modifications that better highlight how the symmetry of the bilayer affects the GSFE. First, we define two parameters, $(v, w) \in [0, 2\pi] \times [0, 2\pi]$, which describe $\mathbf{b}(\mathbf{r})$ in terms of the unit-cell vectors. For the bilayers studied here, v and w are related to the stacking vector (b_x, b_y) by

$$\begin{pmatrix} v \\ w \end{pmatrix} = \frac{2\pi}{\alpha} \begin{bmatrix} 1 & -1/\sqrt{3} \\ 0 & 2/\sqrt{3} \end{bmatrix} \begin{pmatrix} b_x \\ b_y \end{pmatrix}. \tag{3}$$

The GSFE can then be written in a relatively simple form in the (v, w) basis:

$$\begin{aligned} V_{\text{GSFE}} = c_0 &+ c_1(\cos v + \cos w + \cos(v+w)) \\ &+ c_2(\cos(v+2w) + \cos(v-w) + \cos(2v+w)) \\ &+ c_3(\cos(2v) + \cos(2w) + \cos(2v+2w)) \\ &+ c_4(\sin v + \sin w - \sin(v+w)) \\ &+ c_5(\sin(2v+2w) - \sin(2v) - \sin(2w)) \end{aligned} \tag{4}$$

with the coefficients $c_0, \ldots, c_5$ given in Table I. For hexagonal systems like graphene that have symmetry be-

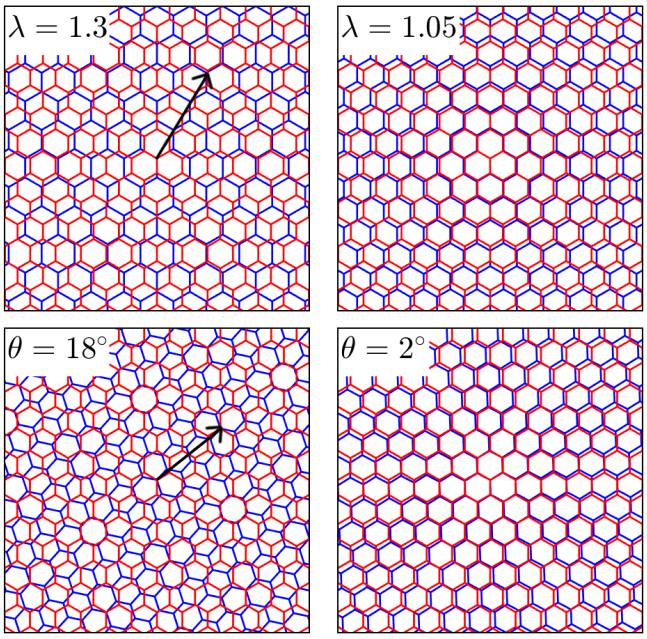

FIG. 2. Examples of misaligned lattices. Top panels show bilayers whose lattice constants differ by factor of λ while the bottom panels show bilayers with relative twist angle θ. The left panels show misaligned structures with small moiré length (moiré wavelength given by the black arrow), while the right panels show nearly-aligned structures with large moiré length.

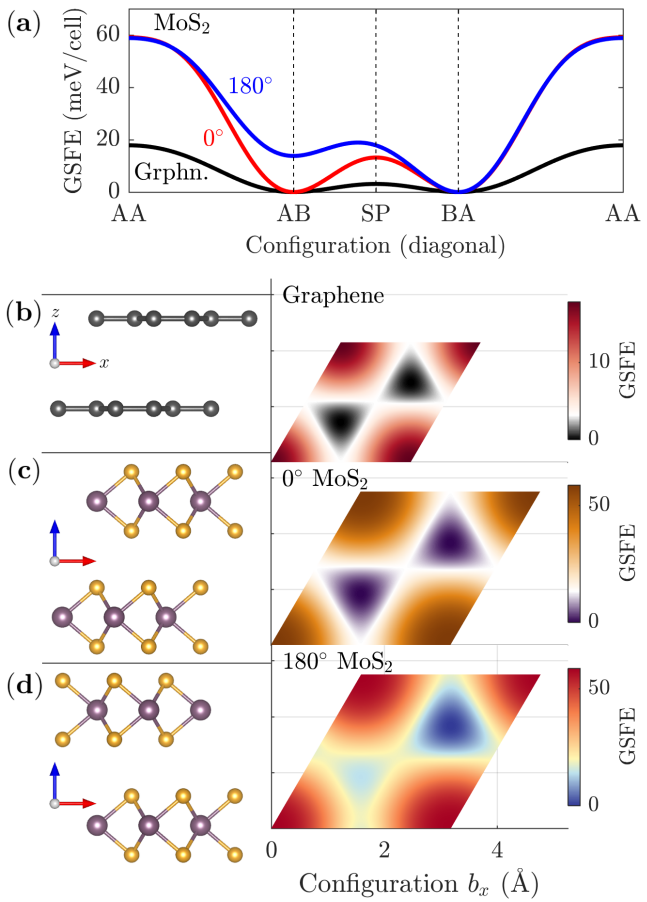

FIG. 3. **(a)**: The Generalized Stacking Fault Energy (GSFE) evaluated on stackings sampled along the unit-cell diagonal for three different bilayers. **(b)**,**(c)**,**(d)**: Side-views of the ground-state stacking orientation for each bilayer, and corresponding GSFE dependence on configurations in the unit-cell Γ. The color scale in each case is chosen to make the saddle point (SP) energy white or bright yellow.

tween the AB and BA stackings, the coefficients of the sine terms are constrained to be zero as the GSFE functional must be even around the origin (AA stacking).

There is always a lowest-energy stacking between layers, and relaxation should distort the layers to maximize the area of that stacking (or stackings, in the case of degenerate ground states). Examples of bilayers under lattice mismatches (λ) and twists (θ), are displayed in Fig. 2. When the lattices are nearly alligned, only small amounts of lattice straining are necessary to form a large area of uniform stacking. As the misalignment increases the strain needed for creating uniform stacking grows larger, making domain formation less favorable. To understand the stacking energy landscape of layered materials, we show the GSFE for graphene and the two high-symmetry stacking orientations of MoS_2 (0° and 180° rotation between layers) in Fig. 3. The two different orientations in bilayer MoS_2 are due to the presence of different atomic species (Mo and S) on the two sub-lattices of the honeycomb lattice. The 0° MoS_2 bilayer has two identical low-energy stackings, similar to graphene, while the 180° MoS_2 bilayer has only one low-energy stacking. Symmetry arguments can predict the critical points of the GSFE, and their relative energies can be ranked by comparing interlayer distances between atoms at each stacking. Our use of the GSFE for interlayer interactions is expected to be more accurate than empirical atomistic potentials when they exist (for materials like graphene and hBN)[33], and allows for modeling of bilayers where no such potentials exist to our knowledge (e.g., MoS_2).

This modeling strategy works best when the twist angle is close to the one used to fit the GSFE (0°) and we do not recommend using the functionals provided here for studying relaxations at angles larger than 10°. For larger angles, one should find a commensurate supercell that is closer to the angle of interest, and then treat the corresponding bilayer supercell as an effective untwisted unit cell. The strain energy and GSFE functional for this enlarged cell can be readily obtained. If the supercell has many atoms, the GSFE is likely very smooth and does not lead to appreciable domain formation. However, near angles that form small supercells, such as 21.78° for twisted honeycomb lattices, the GSFE may still have enough structure to show domain formation. We leave such investigation to future work.

Since the stacking configurations of untwisted layers gives a clear picture of the bilayer energetic landscape,

Material	K	G	c_0	c_1	c_2	c_3	c_4	c_5
Graphene	69,518	47,352	6.832	4.064	-0.374	-0.095	0.000	0.000
0° MoS_2	49,866	31,548	27.332	14.02	-2.542	-0.884	0.000	0.000
180° MoS_2	49,866	31,548	30.423	12.322	-2.077	-0.783	2.397	0.259

TABLE I. Coefficients for the strain energy and Fourier components of the GSFE in bilayer graphene and the two high-symmetry forms of bilayer MoS_2. All values are in units of meV per unit-cell.

framing the relaxation problem entirely in terms of configurations may prove useful. The collection of all local stackings in an incommensurate system forms a dense compact domain called configuration space[34–36], and we now outline its construction. We define 2×2 matrices A_1 and A_2 as the Bravais lattice vectors of layer 1 and layer 2, whose unit-cells are labeled as Γ_1 and Γ_2. Any point in the Bravais lattice of layer 2 is indexed by an integer tuple, $\mathbf{n}\in\mathbb{Z}^2$, and it will have position $\mathbf{r}=A_2\mathbf{n}$. We can compute its stacking configuration relative to layer 1 by $\mathbf{b}_2 : A_2\mathbb{Z}^2 \to \Gamma_1$ explicitly by $\mathbf{b}_2(A_2\mathbf{n}) = A_2\mathbf{n} = \mathbf{r}(\mathbf{n})$. Although the function $\mathbf{b}_2$ lacks an explicit modulation in its definition, it is implicitly periodic over the torus Γ_1. As defined, $\mathbf{b}_2$ would vary quickly on the scale of the unit-cell if $\mathbf{r}$ is formally substituted for $\mathbf{r}(\mathbf{n})$. This is not desirable, so instead we smoothly interpolate $\mathbf{b}_2(\mathbf{r}(\mathbf{n}))$ between lattice points. We define lattice mismatch matrices that encode the effective moiré pattern: $1-A_1A_2^{-1}=A_{\delta 2}$ and $1-A_2A_1^{-1}=A_{\delta 1}$, which yield interpolated mappings

$$\begin{aligned} &\mathbf{b}_2(A_2\mathbf{n}) = (1-A_1A_2^{-1})A_2\mathbf{n} \\ \implies &\mathbf{b}_2(\mathbf{r}) \equiv A_{\delta 2}\mathbf{r}, \quad \mathbf{b}_1(\mathbf{r}) \equiv A_{\delta 1}\mathbf{r} \end{aligned} \tag{5}$$

where $\mathbf{b}_i(\mathbf{r})$ will vary slowly on the atomic length scale and should be considered modulo the unit cell torus of the opposite layer. There is also a relationship between atomic displacements in configuration space, $\mathbf{u}_i(\mathbf{b}_i)$, and those in real space:

$$\mathbf{U}_i(\mathbf{r}) = \mathbf{u}_i(A_{\delta i}\mathbf{r}) \implies \nabla\mathbf{U}_i = \nabla\mathbf{u}_i A_{\delta i}. \tag{6}$$

Each $\mathbf{u}_i$ is periodic over the unit cell of the *opposite* layer, e.g. $\mathbf{u}_1$ is periodic on Γ_2. In this way $\mathbf{u}_i$ represents a regular sampling of the atoms that make up layer i, whereas conventional continuum real space approaches sample $\mathbf{U}_i(\mathbf{r})$ on a mesh of positions. This difference allows $\mathbf{u}_i$ to accurately reproduce incommensurate relaxed atomistic structures where purely real space approaches are ill-suited. $A_{\delta i}$ can be interpreted as a map from real space to configuration space, and $A_{\delta i}^{-1}$ as the inverse map. This transformation has been done in previous work for studying electronic structure in incommensurate materials[34,37], and here it allows for relaxation of incommensurate bilayers.

To calculate relaxation for twisted bilayers in configuration space, the energy functionals must be defined over the configuration space $\{\Gamma_1,\Gamma_2\}$. As each Γ_i is the unit cell torus independent of twist angle, the configuration space remains periodic and compact even when the bilayer is incommensurate in real space. Throughout the energy functionals, the real space displacement fields $\mathbf{U}_i(\mathbf{r})$ must be replaced by the configuration space displacement fields $\mathbf{u}_i(\mathbf{b}_i)$. This substitution assumes that if two atoms on layer 2 have similar stacking relative to layer 1, then they must have similar relaxation. For two arbitrary lattices, with the GSFE computed over Γ_1, the total energy is given as:

$$\begin{aligned} E_{\text{tot}}(\mathbf{u}_1,\mathbf{u}_2) &\equiv E_{\text{inter}}(\mathbf{u}_1,\mathbf{u}_2) + \sum_{i=1}^{2} E^{(i)}_{\text{intra}}(\nabla\mathbf{u}_i) \\ E^{(i)}_{\text{intra}}(\nabla\mathbf{u}_i) &= \int_{\Gamma_{\tilde{i}}} \frac{1}{2}\left(\mathcal{E}_c(\nabla\mathbf{u}_i)\; C_i\; \mathcal{E}_c(\nabla\mathbf{u}_i)\right) d\mathbf{b}_{\tilde{i}} \\ \mathcal{E}_c(\nabla\mathbf{u}_i) &= \frac{1}{2}\left(\nabla\mathbf{u}_i A_{\delta i} + A_{\delta i}^T\nabla\mathbf{u}_i^T\right) \\ E_{\text{inter}}(\mathbf{u}_1,\mathbf{u}_2) &= \int_{\Gamma_1} V_{\text{GSFE}}(\mathbf{b}_2+\mathbf{u}_2(\mathbf{b}_2)-\tilde{\mathbf{u}}_1(\mathbf{b}_2))d\mathbf{b}_2 \\ \tilde{\mathbf{u}}_1(\mathbf{b}_2) &\equiv \mathbf{u}_1(-A_2A_1^{-1}\mathbf{b}_2) \end{aligned} \tag{7}$$

where $\Gamma_{\tilde{i}}$ is the unit cell of the layer opposite layer i. The total interlayer coupling is described by a single integral evaluation of V_{GSFE} over the configuration space of only one layer. This works well if the two layers have similar unit cells. Alternatively, the interlayer coupling can be split into two equal components of $\frac{1}{2}V_{\text{GSFE}}$ for each Γ_i. This introduces additional complexity in the twisted case, as the relative orientations between the twisted Γ_i's needs to be taken into account.

To illustrate how to transform the relaxation problem to configuration space, we focus on a bilayer system with small twist-angle θ. Letting layer 2 be rotated counterclockwise by θ relative to layer 1 gives $A_2 = R_\theta A_1$ with R_θ the conventional rotation matrix. Then $A_{\delta 1} = 1-R_\theta^{-1}$ and $A_{\delta 2} = 1-R_\theta$, and we can expand the rotation matrix to first order in θ to get $\mathbf{b}_i(\mathbf{r})$:

$$\mathbf{b}_2(\mathbf{r}) \approx \theta\begin{pmatrix}-r_y\\ r_x\end{pmatrix}, \quad \mathbf{b}_1(\mathbf{r}) \approx \theta\begin{pmatrix}r_y\\ -r_x\end{pmatrix}. \tag{8}$$

Substituting this approximation for $A_{\delta i}$ into Eq. (7) also shows how the gradient of $\mathbf{u}_i$ contributes to the

strain-energy $\mathcal{E}_c$ with a factor of θ. This scaling predicts that as $\theta \to 0$, eventually $\mathbf{u}_i$ can balance the intralayer and interlayer energies by forming strain solitons. The width of the domain walls in configuration space should diminish like θ, resulting in constant real space width.

To further simplify the model in the case of twisted bilayers, notice that V_{GSFE} depends only on the difference of atomic displacements $\Delta\mathbf{u} \equiv \mathbf{u}_2 - \tilde{\mathbf{u}}_1$. If we consider a bilayer system where layer 1 is frozen and only layer 2 can relax, we have $\mathbf{u}_1 = 0$ and $\Delta\mathbf{u} = \mathbf{u}_2$. As $\Delta\mathbf{u}$ minimizes the total stacking energy, when relaxing both layers we want to obtain a similar $\Delta\mathbf{u}$ while minimizing the strain energy. The two unit cells are nearly identical, so the true solution is one that splits $\Delta\mathbf{u}$ equally between the two layers. This can be done by setting a single $\mathbf{u}$ field $\mathbf{u} \equiv \mathbf{u}_2 = -\tilde{\mathbf{u}_1}$ over a single $\Gamma \equiv \Gamma_1$, leading to a total energy functional:

$$E_{\mathrm{tot}}(\mathbf{u}) = \frac{1}{|\Gamma|}\int_{\Gamma}\left[2\mathcal{E}_{\mathrm{intra}}(\nabla\mathbf{u}) + V_{\mathrm{GSFE}}(b + 2\mathbf{u})\right]d\mathbf{b}. \quad (9)$$

For the three bilayers studied here, there is also a mirror-plane symmetry along the vertical plane that bisects the twist-angle, which we will label S. This symmetry gives the relation $u = Su(Sb)$ as an additional constraint during any optimization procedure. We minimize the total energy given in Eq. (9) with a standard optimization routine implemented in the Optim Julia package[38] after uniformly sampling configuration space with a discrete Fourier basis of plane-waves. This yields the smooth displacement field in configuration space corresponding to the ground state of the relaxed bilayer system. The result can then be mapped to real space for use in other applications (for example, electronic structure calculation) with Eq. (6).

In summary, this method makes four approximations to arrive at a greatly simplified configuration space continuum model: (1) the in-plane and interlayer coupling energies are well fitted by the strain moduli and GSFE functionals of the untwisted bilayer; (2) short range symmetry-breaking relaxations are ignored; (3) the relaxation pattern for any configuration can be smoothly interpolated by sampling nearby configurations (e.g. a smooth and quasi-periodic deformation field in space); (4) the bilayer is made of homogeneous layers, allowing for the relaxation of both layers to be related to a single layer's relaxation by symmetry (only needed if one wishes to simplify the energy functional).

To illustrate the general nature of domain formation in incommensurate graphene and TMDC bilayers, we wish to show domain-wall formation on a scale where both the unit-cell and the moiré supercell are easily visible. We exaggerate the interlayer coupling by increasing V_{GSFE} by a factor of 100 for $\theta = 3^\circ$ twisted bilayers of graphene and 180° MoS_2 in Fig. 4. For both systems, relaxation causes the regions of lowest energy stackings to expand in configuration space and the higher energy stackings to reduce in size, producing thin lines and nodes. In real space, this means the bilayers form large domains of uniform stacking surrounded by thin solitons which intersect at "pinned" high-energy stacking nodes. For bilayer graphene and bilayer 0° MoS_2, there are two identical ground state stackings, commonly refered to as the AB and BA stackings. These stackings are equal in energy and compete to create a tiling of AB and BA triangular domains as observed in dark-field imaging studies of twisted bilayer graphene[6,9]. For 180° bilayer MoS_2, there is only one low-energy stacking. It expands and causes the formation of hexagonal domains.

Furthermore, due to the anti-symmetric nature of $b(\mathbf{r})$ in Eq. (8), $\nabla \times \mathbf{U}(\mathbf{r}) \approx \theta\,(\nabla \cdot \mathbf{u}(\mathbf{b}))$, that is, the local change in the real space twist angle ($\nabla \times \mathbf{U}$) caused by the relaxation can be computed by taking the divergence of the configuration space displacement field. The low-energy stackings have $\nabla \cdot \mathbf{u} < 0$, which implies an "untwisting" of those areas in real space. Meanwhile, the high energy stackings have $\nabla \cdot \mathbf{u} > 0$, which implies additional twisting. This is why the domains show almost no local twist angle in real space, while the high-energy nodes are twisted more. We find that the local twist angle at the AA stacking in twisted bilayer graphene converges to 1.7° as the global twist angle approaches 0°, which agrees with the results of a recent real space approach[9].

At small twist angles, large domains that have 0° local twist angle can appear. This is related to the commensurate-incommensurate transition that occurs in nearly-aligned bilayers, such as the graphene-hBN system with lattice size mismatch[7]. The commensurate-incommensurate transition, which would cause a discontinuity in our configuration space model, has been studied rigorously but is only well understood in the one-dimensional case under certain assumptions (the Frenkel-Kontorova model)[39]. A discussion of how our method relates to the Frenkel-Kontorova model is presented in our formal study of the mathematical problem[35].

To show that these phenomena are general, we calculate relaxed structures for various twist angles in Fig. 5. We note that $\mathbf{U}_i(\mathbf{r})$ is aperiodic and captures incommensurate structure even though $\mathbf{u}(\mathbf{b})$ is periodic on Γ. Consequently, the moiré domains in Fig. 4 and 5 cannot be obtained from a supercell approach since they do not exactly repeat. The relaxations for graphene and 0° MoS_2 are almost indistinguishable, except the twist angle needed in 0° MoS_2 is roughly twice what is needed in graphene for a comparable relaxed structure. For all three structures, the strain solitons and nodes shrink in configuration space proportionally to the twist-angle. As translating the relaxation in configuration space to real space involves a factor of θ^{-1}, the shape of solitons and nodes in real space are unaffected by the twist angle at sufficiently small angles. This is expected, as there is an optimal width for a strain soliton. As the twist angle decreases the walls do not change in width, but only in their length as the domains become larger.

When considering multilayer systems, where the num-

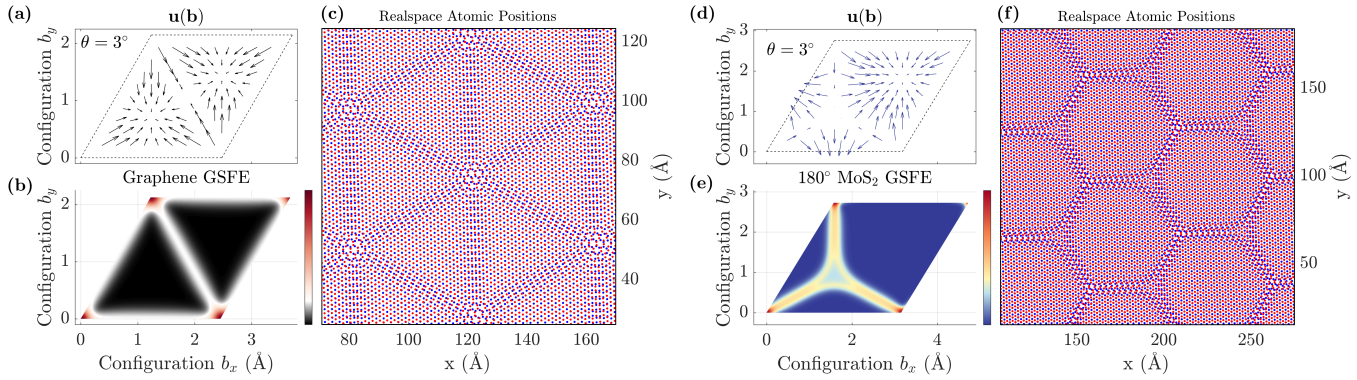

FIG. 4. Relaxation for a graphene and 180° MoS_2 bilayer with a 3° relative twist. Interlayer coupling was amplified by a factor of 100 for easy visualization. **(a)**: The graphene displacement field $\mathbf{u}$ over Γ. **(b)**: $V_{\mathrm{GSFE}}(\mathbf{b}+2\mathbf{u}_1(\mathbf{b}))$ over Γ that shows the moiré pattern in configuration space for graphene. **(c)**: The graphene atomistic positions after applying the displacement fields. **(d)**,**(e)**,**(f)** are the corresponding plots for MoS_2

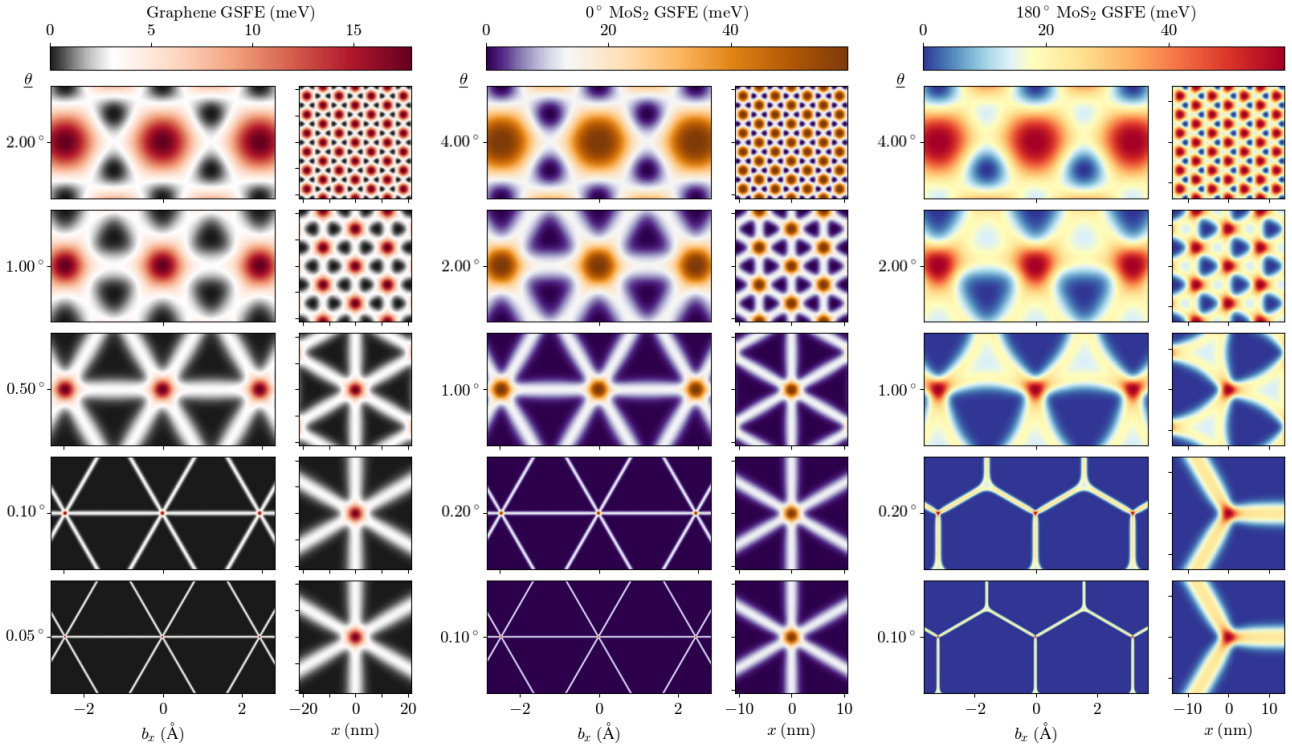

FIG. 5. Configuration relaxation results for twisted bilayers with five incommensurate twist angles each. The left panel of each column shows $V_{\mathrm{GSFE}}(\mathbf{b}+2\mathbf{u}(\mathbf{b}))$ over Γ (the relaxation pattern in configuration space) and the right panel shows $V_{\mathrm{GSFE}}(\mathbf{r})$ (over real space).

ber of layers p is greater than two, this formalism generalizes but produces a more difficult PDE. In a p-layered system, each layer has $p-1$ unique configurations with respect to other layers. Therefore, the configuration space is a $2(p-1)$ dimensional torus[21]. The configuration space can still be sampled using a uniform mesh, and the interlayer stacking energy is easy to evaluate once one has defined the proper interpolation scheme given the system geometry. The intralayer strain energy is less straightforward as the in-plane connections between lattice sites span a 2-dimensional submanifold of the $2(p-1)$-dimensional torus. This strain energy, although not impossible to implement, makes the resulting PDE non-elliptic and may be difficult to properly optimize. For additional information, please see Ref. 21.

In conclusion, we have presented an approach for

modeling relaxations in incommensurate systems. The methodology, based on treating the incommensurate system consistently, has led to identification of key physical ingredients for predicting what relaxations may occur. If the lattices are aligned close to a commensurate angle which yields a small cell, large-scale domain-wall formation is expected. As the lattices are twisted away from such an angle, the domains will become smaller and their boundaries less sharp until almost no relaxation occurs at large misalignment. The geometry of the domains and walls is determined by the number and nature of the critical points in the interlayer energy functional, and their domain size scales with the twist angle. This naturally creates regular patterns of uniformly stacked bilayers divided by thin strain solitons. If the bilayer geometry encodes important topological information for electrons, or if the strain and sharp stacking potentials act as a useful source of electron confinement, small twist angles can create regular networks of confined 1D states which are easily realized in experiment.

ACKNOWLEDGMENTS

We acknowledge H. Yoo, R. Engelke, P. Kim, S. Fang, and K. Zhang for helpful discussions. Calculations were performed on the Odyssey cluster supported by the FAS Division of Science, Research Computing Group at Harvard University. This work was supported by the ARO MURI Award No. W911NF-14-0247. S.B.T. is supported by the Department of Energy Computational Science Graduate Fellowship.

[1] G. A. Tritsaris, S. N. Shirodkar, E. Kaxiras, P. Cazeaux, M. Luskin, P. Plechac, and E. Cances, Journal of Material Research **31**, 959 (2016).
[2] C. R. Dean, L. Wang, P. Maher, C. Forsythe, F. Ghahari, Y. Gao, J. Katoch, M. Ishigami, P. Moon, M. Koshino, T. Taniguchi, K. Watanabe, K. L. Shepard, J. Hone, and P. Kim, Nature **497**, 598 EP (2013).
[3] B. Hunt, J. D. Sanchez-Yamagishi, A. F. Young, M. Yankowitz, B. J. LeRoy, K. Watanabe, T. Taniguchi, P. Moon, M. Koshino, P. Jarillo-Herrero, and R. C. Ashoori, Science **340**, 1427 (2013), http://science.sciencemag.org/content/340/6139/1427.full.pdf.
[4] A. K. Geim and I. V. Grigorieva, Nature **499**, 419 (2013).
[5] C. Zhang, C.-P. Chuu, X. Ren, M.-Y. Li, L.-J. Li, C. Jin, M.-Y. Chou, and C.-K. Shih, Science Advances **3** (2017), 10.1126/sciadv.1601459, http://advances.sciencemag.org/content/3/1/e1601459.full.pdf.
[6] J. S. Alden, A. W. Tsen, P. Y. Huang, R. Hovden, L. Brown, J. Park, D. A. Muller, and P. L. McEuen, Proceedings of the National Academy of Sciences **110**, 11256 (2013), http://www.pnas.org/content/110/28/11256.full.pdf.
[7] C. R. Woods, L. Britnell, A. Eckmann, R. S. Ma, J. C. Lu, H. M. Guo, X. Lin, G. L. Yu, Y. Cao, R. V. Gorbachev, A. V. Kretinin, J. Park, L. A. Ponomarenko, M. I. Katsnelson, Y. N. Gornostyrev, K. Watanabe, T. Taniguchi, C. Casiraghi, H.-J. Gao, A. K. Geim, and K. S. Novoselov, Nature Physics **10**, 451 (2014).
[8] N. N. T. Nam and M. Koshino, Phys. Rev. B **96**, 075311 (2017).
[9] K. Zhang and E. B. Tadmor, Journal of the Mechanics and Physics of Solids **112**, 225 (2018).
[10] H. Kumar, L. Dong, and V. B. Shenoy, Scientific Reports **6** (2016), article.
[11] M. Yankowitz, J. I.-J. Wang, A. G. Birdwell, Y.-A. Chen, K. Watanabe, T. Taniguchi, P. Jacquod, P. San-Jose, P. Jarillo-Herrero, and B. J. LeRoy, Nature Materials **13** (2014).
[12] P. San-Jose, R. V. Gorbachev, A. K. Geim, K. S. Novoselov, and F. Guinea, Nano Letters **14**, 2052 (2014), pMID: 24605877, https://doi.org/10.1021/nl500230a.
[13] A. Vaezi, Y. Liang, D. H. Ngai, L. Yang, and E.-A. Kim, Phys. Rev. X **3**, 021018 (2013).
[14] L.-J. Yin, H. Jiang, J.-B. Qiao, and L. He, Nature Communications **7**, 11760 EP (2016), article.
[15] B.-Y. Jiang, G.-X. Ni, Z. Addison, J. K. Shi, X. Liu, S. Y. F. Zhao, P. Kim, E. J. Mele, D. N. Basov, and M. M. Fogler, Nano Letters **17**, 7080 (2017), pMID: 28967761, https://doi.org/10.1021/acs.nanolett.7b03816.
[16] P. Rickhaus, J. Wallbank, S. Slizovskiy, R. Pisoni, H. Overweg, Y. Lee, M. Eich, M.-H. Liu, K. Watanabe, T. Taniguchi, T. Ihn, and K. Ensslin, Nano Letters **0**, null (0), pMID: 30336041, https://doi.org/10.1021/acs.nanolett.8b02387.
[17] S. Huang, K. Kim, D. K. Efimkin, T. Lovorn, T. Taniguchi, K. Watanabe, A. H. MacDonald, E. Tutuc, and B. J. LeRoy, Phys. Rev. Lett. **121**, 037702 (2018).
[18] D. K. Efimkin and A. H. MacDonald, Phys. Rev. B **98**, 035404 (2018).
[19] P. San-Jose, A. Gutiérrez-Rubio, M. Sturla, and F. Guinea, Phys. Rev. B **90**, 075428 (2014).
[20] M. Yankowitz, K. Watanabe, T. Taniguchi, P. San-Jose, and B. J. LeRoy, Nature Communications **7**, 13168 EP (2016), article.
[21] P. Cazeaux, M. Luskin, and D. Massatt, ArXiv e-prints 1806.10395 (2018), arXiv:1806.10395 [physics.comp-ph].
[22] C. R. Dean, A. F. Young, I. Meric, C. Lee, L. Wang, S. Sorgenfrei, K. Watanabe, T. Taniguchi, P. Kim, K. L. Shepard, and J. Hone, Nature nanotechnology **5**, 722 (2010).
[23] E. Kaxiras and M. S. Duesbery, Phys. Rev. Lett. **70**, 3752 (1993).
[24] J. R. Rice and G. E. Beltz, Journal of the Mechanics and Physics of Solids **42**, 333 (1994).
[25] U. V. Waghmare, V. Bulatov, E. Kaxiras, and M. S. Duesbery, Philosophical Magazine A **79**, 655 (1999), https://doi.org/10.1080/01418619908210323.
[26] U. V. Waghmare, E. Kaxiras, and M. Duesbery, physica status solidi (b) **217**, 545 (2000).
[27] S. Zhou, J. Han, S. Dai, J. Sun, and D. J. Srolovitz, Phys. Rev. B **92**, 155438 (2015).
[28] S. Dai, Y. Xiang, and D. J. Srolovitz, Nano Letters **16**, 5923 (2016), pMID: 27533089, https://doi.org/10.1021/acs.nanolett.6b02870.
[29] G. Kresse and J. Hafner, Phys. Rev. B **47**, 558 (1993).

[30] G. Kresse and J. Furthmüller, Phys. Rev. B **54**, 11169 (1996).
[31] J. Klimes, D. R. Bowler, and A. Michaelides, Phys. Rev. B **83**, 195131 (2011).
[32] H. Peng, Z.-H. Yang, J. P. Perdew, and J. Sun, Phys. Rev. X **6**, 041005 (2016).
[33] A. N. Kolmogorov and V. H. Crespi, Phys. Rev. B **71**, 235415 (2005).
[34] D. Massatt, M. Luskin, and C. Ortner, Multiscale Modeling and Simulation **15**, 476 (2017).
[35] P. Cazeaux, M. Luskin, and E. Tadmor, SIAM J. Multiscale Modeling & Simulation **15**, 56 (2017).
[36] E. Cancès, P. Cazeaux, and M. Luskin, Journal of Mathematical Physics **58**, 063502 (23pp) (2017).
[37] S. Carr, D. Massatt, S. Fang, P. Cazeaux, M. Luskin, and E. Kaxiras, Phys. Rev. B **95**, 075420 (2017).
[38] P. K. Mogensen and A. N. Riseth, Journal of Open Source Software **3**, 615 (2018).
[39] S. Aubry and P. L. Daeron, Physica D: Nonlinear Phenomena **8**, 381 (1983).